Mineralium Deposita (2002) 37: 772–781
DOI 10.1007/s00126-002-0317-0

LETTER

Alain Cheilletz · Gilles Levresse · Dominique Gasquet
Moulay Rachid Azizi-Samir · Rachid Zyadi
Douglas A. Archibald · Edward Farrar

The giant Imiter silver deposit: Neoproterozoic epithermal mineralization in the Anti-Atlas, Morocco

Received: 8 November 2001 / Accepted: 14 May 2002 / Published online: 9 August 2002

Abstract The world-class Imiter silver deposit, in the Anti-Atlas Mountains of Morocco, is a Neoproterozoic epithermal vein deposit genetically associated with a felsic volcanic event, and formed within a regional extensional tectonic regime. Rhyolitic volcanism related to ore formation has been dated at 550 ± 3 Ma by ion-probe U/Pb on zircons. The economic silver mineralization is superimposed on an older, discrete base-metal assemblage associated with calc-alkaline granodioritic magmatism. The magmatism is dated at 572 ± 5 Ma by ion-probe U/Pb dating on zircons, and by $^{40}Ar/^{39}Ar$ dating on hydrothermal muscovites. In the Anti-Atlas Mountains, the Precambrian–Cambrian transition appears as an important period for the formation of major, productive precious-metal deposits associated with volcanic events and extensional tectonics. The Imiter silver deposit constitutes a Precambrian analogue to modern epithermal deposits.

Keywords Epithermal · Silver · Extensional tectonics · Geochronology · Neoproterozoic · Morocco

Introduction

The Imiter deposit is located in the Anti-Atlas Mountains, Morocco, northern Africa (Fig. 1). It is one of the largest silver deposits in the world, with currently identified resources of 8,000 metric tonnes (t) metal. To explain the origin of this huge silver concentration, multistage genetic models have been invoked during the last 30 years (Leistel and Qadrouci 1991; Barodi et al. 1998; Baroudi et al. 1999), mainly involving an originally syngenetic deposit (Vargas 1983; Popov et al. 1986; Guillou et al. 1988; Popov 1995) and various stages of epigenetic remobilization. The mineralization is controlled by the 7-km-long, Imiter normal fault zone (Leistel and Qadrouci 1991; Ouguir et al. 1994; Fig. 2) which offsets the Neoproterozoic (PII, following the regional terminology) metasedimentary black shale and greywacke series and the late Neoproterozoic (PIII) volcanic rock succession. The mined ore includes (1) Ag–Hg amalgams (with locally as much as 40% Hg), (2) pure native silver represented by spectacular plates weighing as much as 100 kg, (3) silver sulfosalts which include imiterite ($HgAg_2S_2$; Guillou et al. 1985), and (4) various As–Pb–Zn–Co–Ni sulfide minerals. Most of the native silver has been attributed to supergene enrichment processes. The hypothesized lower depth of the economic mineralization was about 300 m (Vargas 1983; Popov et al. 1986; Popov 1995). However, a recent drill hole encountered the silver-rich amalgam at 540 m below the surface, demonstrating continuation of the ore to greater depth. Comparison with other similar silver deposits in the world, particularly those belonging to the epithermal type, was briefly evoked by Leistel and Qadrouci (1991) and Baroudi et al. (1999) and,subsequently,more definitively presented by Cheilletz et al. (2000), Levresse (2001) and Levresse et al. (2001a, 2001b).

Although the role of the Imiter fault in the localization of the silver mineralization is now well-established, its genetic and geochronological relationships to the ore-forming events and spatially associated magmatism are poorly known. This study provides new field, petrographic, microtectonic and geochronological data which further define the epithermal genetic model. This has important implications at a regional scale, describing favorable conditions for other world-class precious-metal deposits which may exist elsewhere in the Anti-Atlas Mountains. The results collected in the study of the Imiter deposit could help decipher the distribution pattern in space and time of precious-metal systems throughout this area, especially in regions where the late Neoproterozoic–Paleozoic transition is observed (Azizi-Samir et al. 2001; Cheilletz and Gasquet 2001).

Editorial handling: A.C. Brown

A. Cheilletz (✉) · G. Levresse · D. Gasquet
Centre de Recherches Pétrographiques et Géochimiques,
CRPG-CNRS and Ecole Nationale Supérieure de Géologie,
BP 20, 54501 Vandoeuvre-les-Nancy cedex, France
E-mail: cheille@crpg.chrs-nancy.fr

M.R. Azizi-Samir · R. Zyadi
REMINEX – groupe ONA, 26 Av. Allal El Fassi,
Tissir 36–40, Marrakech, Maroc

D.A. Archibald · E. Farrar
Geological Sciences, Queen's University,
Kingston K7L 3N6, Ontario, Canada

Geological setting

The Imiter deposit is located on the northern side of the Saghro massif which constitutes, with the other Proterozoic inliers within early Paleozoic rocks (Ifni, Kerdous, Akka, Sirwa, Ougnat), the Anti-Atlas orogenic belt of Morocco (Fig. 1). The Pan-African Anti-Atlas orogen along the northern side of the western African craton (Fekkak et al. 2001; Ennih and Liegeois 2002) is characterized by the successive development of an oceanic plateau, island arc and marginal basins (ca. 750 Ma; Clauer at al. 1974). In the Imiter area, the oldest sedimentary rocks are represented by Neoproterozoic sequences of black shales, with intercalations of

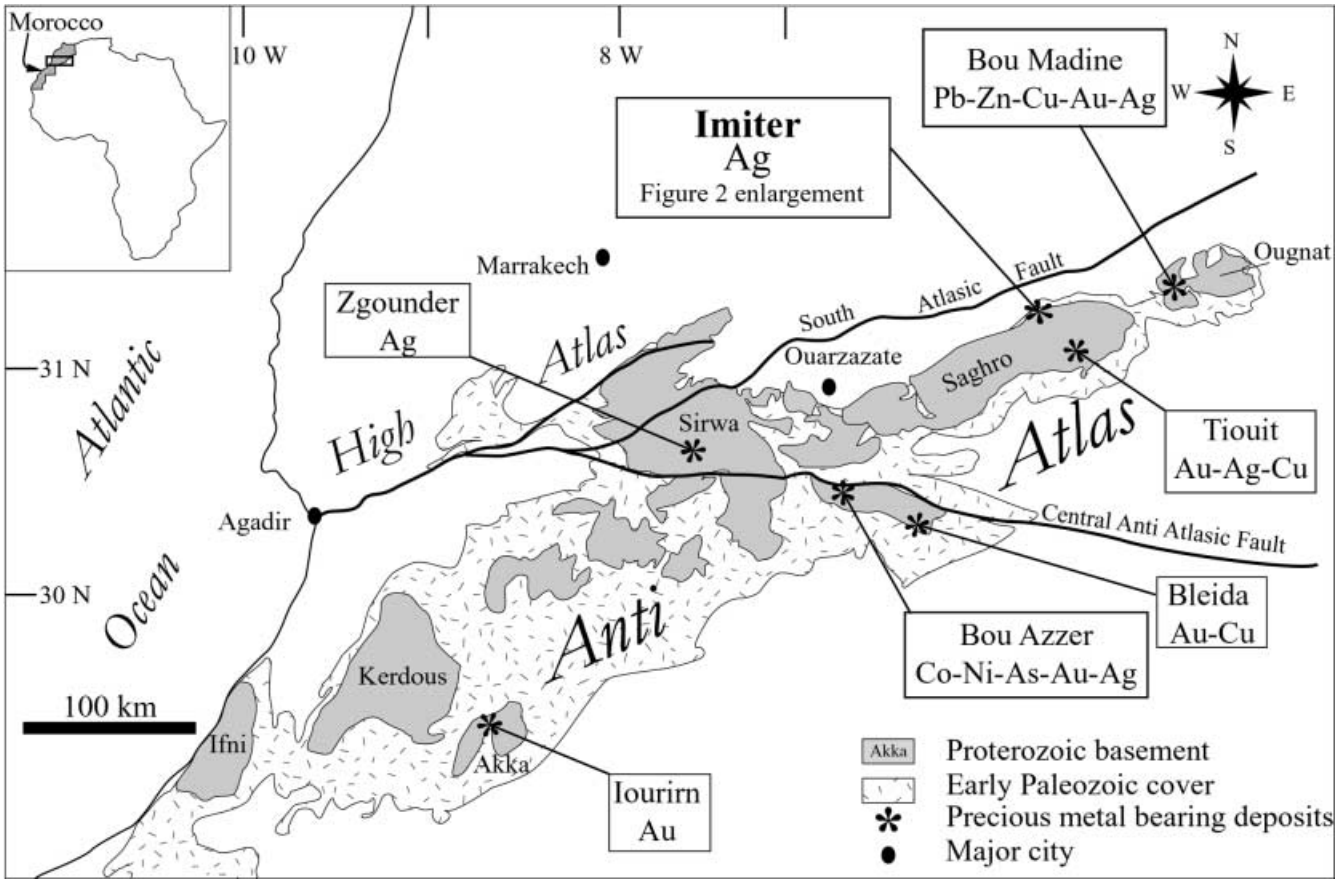

Fig. 1 Major geological units of the Anti-Atlas belt in southern Morocco and location of the Imiter deposit

pyrite-bearing layers interpreted as having formed in an extensional back-arc environment (Ouguir et al. 1996). These rocks were folded and metamorphosed to the lower greenschist facies during the late Neoproterozoic, south-verging arc-continent collision (ca. 680–600 Ma; Leblanc and Lancelot 1980; Villeneuve and Cornée 1994; Fekkak et al. 2000), together with ophiolite emplacement in the Sirwa massif (Gresse et al. 2000). Post-collision evolution is characterized by the continued establishment of an active margin encompassing considerable calc-alkaline magmatism and foreland basin development. In the Imiter area, the metamorphosed black shales are unconformably overlain by an immature basal conglomerate and a late Neoproterozoic volcanic and volcanoclastic sequence, mostly andesitic in composition at its base and ignimbritic at its top. These series, which belong to the locally called "Ouarzazate Group", have been dated at 580–560 Ma (U/Pb on zircons) in the Jbel Bachkoun and Tiouine massifs (Mifdal and Peucat 1985). Granodioritic and granophyric intrusive bodies (Taouzzakt, Igoudrane; Fig. 2) were emplaced during this period of tectonism. In the Anti-Atlas belt, a late Neoproterozoic to Cambrian change records the transition from an active to a passive margin. Associated extension led to rifting, deposition of intercalated clastic and carbonaceous sequences (Adoudou series), and volcanic and subvolcanic magmatism (Piqué et al. 1999).

In the Imiter area, the post-collision evolution of the Anti-Atlas orogen is only partly understood. As noted above, calc-alkaline intrusive rocks are abundant. Associated metamorphic halos in the basement rocks are characterized by a cordierite–andalusite–biotite assemblage at the contact between the black shales and the intrusions (Leistel and Qadrouci 1991). Field relationships define the following intrusive sequence: (1) the Igoudrane granodiorite (Fig. 2) cuts the black shales and is unconformably overlain by the late Neoproterozoic basal conglomerate; (2) the Taouzzakt composite massif, mainly granodioritic in composition and occurring on the western side of the Imiter deposit (Fig. 2), was emplaced into the black shales and the late Neoproterozoic volcanic series; a small granodiorite body, probably related to this massif, occurs under the B3 Hill in underground mine exposures (Fig. 2b, c); and finally (3) a major felsic magmatic event occurred in the Imiter area; it is represented by the Takhatert protrusion to the west and various dikes in the mineralized area, including the major Tachkakacht dike (Fig. 2). Relationships between this last magmatic pulse and the silver mineralization at the Imiter deposit appear to be significant.

The Takhatert intrusion is characterized by a well-defined, concentric magmatic structure (Fig. 2a, b), suggesting that it corresponds to a hypabyssal body emplaced under subaerial conditions. Phenocrysts of K-feldspar, plagioclase and quartz, and a banded whitish glassy matrix give a rhyolitic composition confirmed by chemical analysis (SiO_2 as high as 73.3%, K_2O between 4.7 and 8.0%, and K_2O/Na_2O between 1.7 and 4.4%) and enrichments in low-compatibility elements of a calc-alkaline association. Various dikes of intermediate compositions (mostly trachyandesite) and different relative ages are also present along the Imiter fault zone. In the Igoudrane area, the Tachkakacht rhyolite cuts the north-south-trending trachyandesite dike system.

Middle Cambrian sedimentary rocks, including a basal conglomerate cemented by dolomite, overlie the Neoproterozoic rocks which host the economic silver mineralization. Hercynian and Alpine orogens, although active in various sections of the Anti-Atlas belt, have little effect in the Imiter area.

Mineralization stages and structural control

In the Imiter area, two successive paragenetic episodes have been identified (Fig. 3). An early quartz (Qtz1) vein network is characterized by abundant chlorite (Chl1), muscovite (Ms1) and

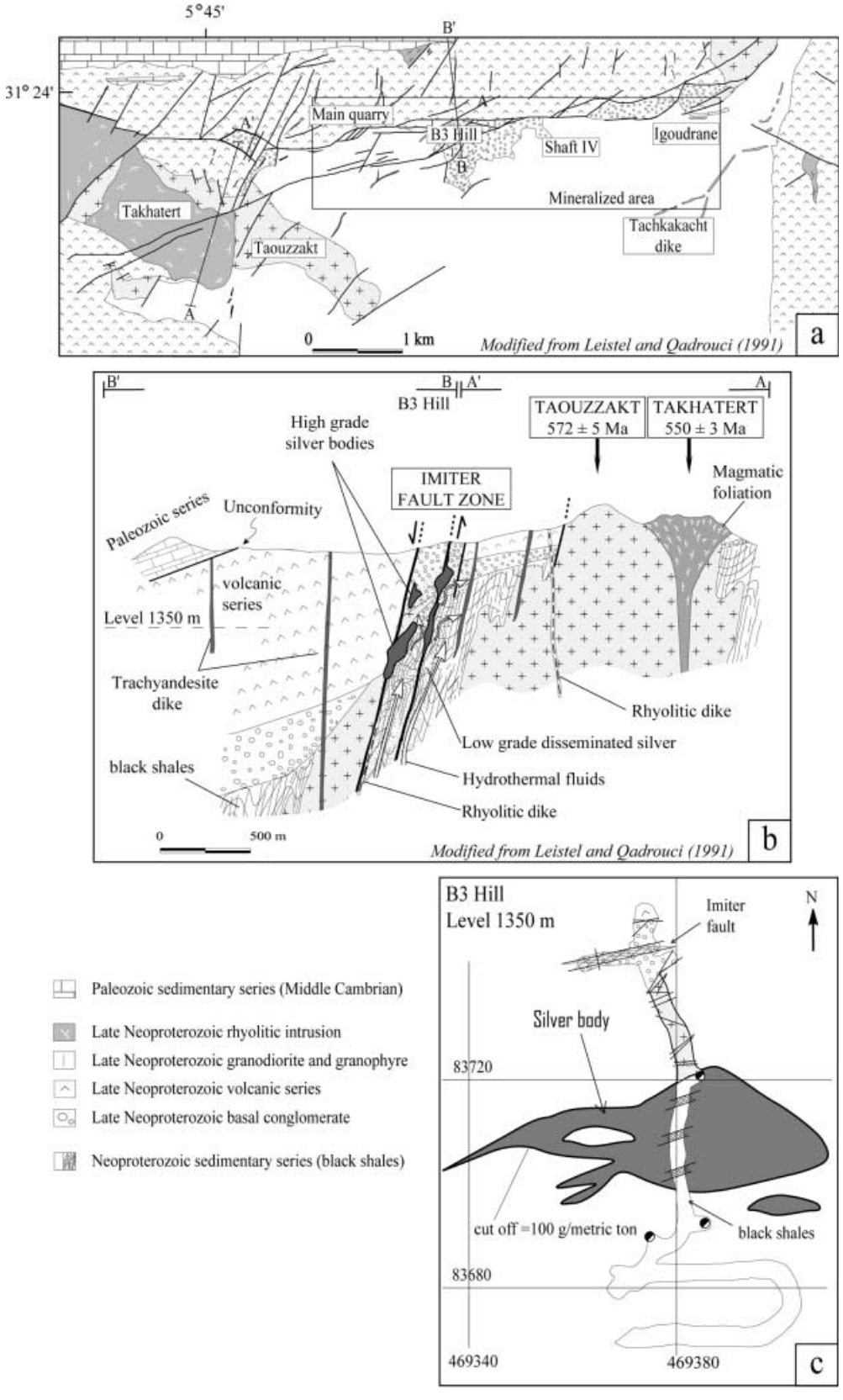

Fig. 2 **a** Geological map of the northern part of the Imiter inlier. **b** Synthesized geological cross section drawn for the *A–A′* and *B–B′* transects. **c** Horizontal projection of a silver body in the B3 Hill workings (1,350 m is the absolute altitude of this mining level)

base-metal sulfide minerals (pyrite, galena and sphalerite with chalcopyrite exsolution; Guillou et al. 1988). This episode, without any silver mineralization, is spatially related to the Taouzzakt granodiorite and will be referenced in the following as the base-

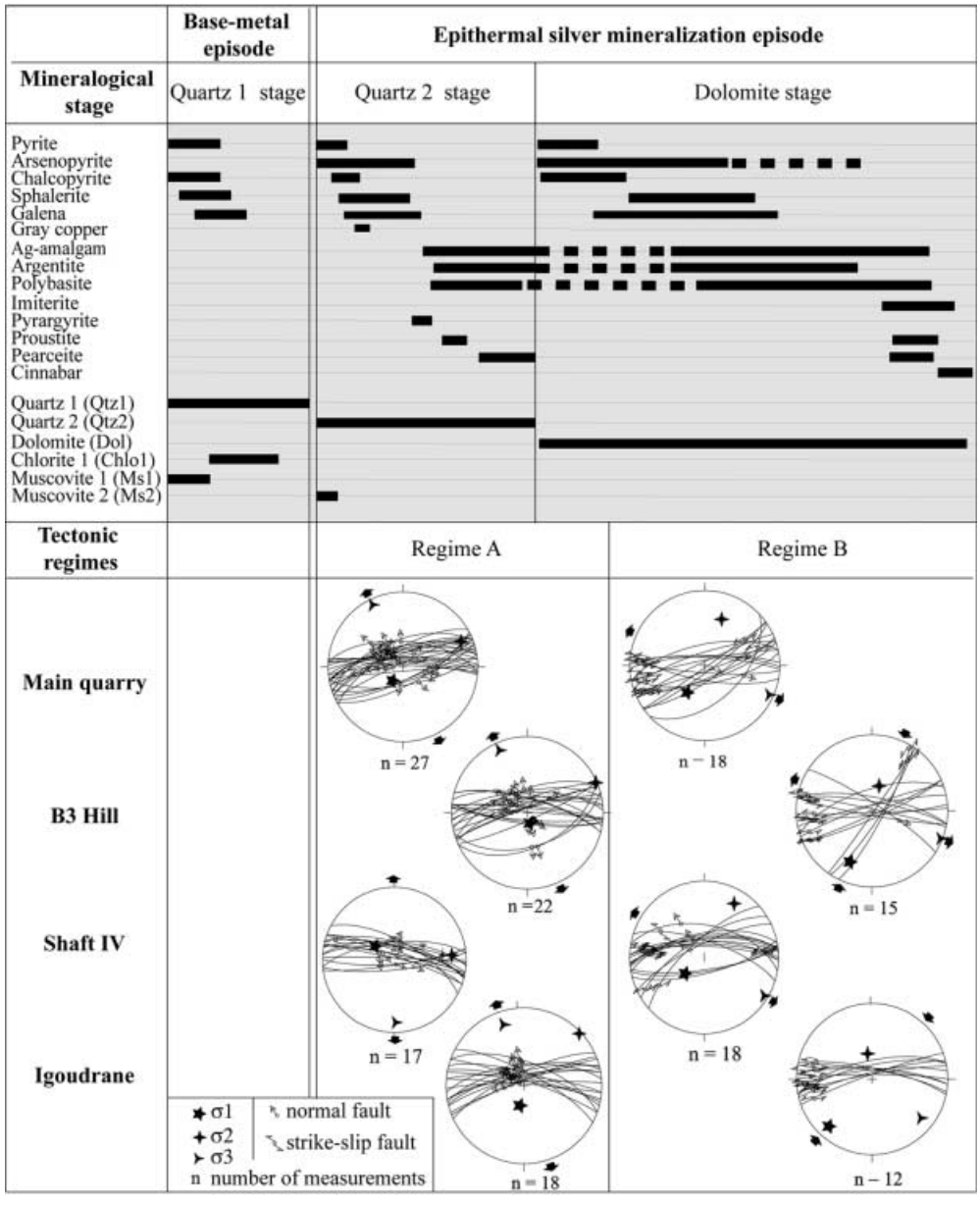

Fig. 3 Paragenetic succession in the Imiter deposit and tectonic regimes during the epithermal silver mineralization episode. The paleostresses ($\sigma 1$, $\sigma 2$, $\sigma 3$) have been estimated using the Angelier and Mechler (1977) method. Note that regime *A* appears predominant and that the changing stress regime (*A* to *B*) is not coupled with a major change in the paragenetic succession, except for a change in gangue from quartz to dolomite

metal episode. The later silver-rich epithermal mineralization episode is subdivided into two stages (Fig. 3). The first stage corresponds to a second generation of quartz veins (gray quartz or Qtz2) with minor muscovite (Ms2) development on Chl1 grains. The second stage is characterized by a pink dolomite gangue and an increasing volume of Co-, Ni-, and Hg-bearing sulfide minerals (including imiterite; Guillou et al. 1985). In the deposit, ore-hosting structures include meter-wide faults, stockwork systems and hydraulic breccias (Fig. 4), along with areas of disseminated silver-bearing minerals within the enclosing Neoproterozoic black shales and volcanic rocks. The main silver orebodies are distributed along the Imiter fault zone. They are represented by irregular columns approximately 10 m wide, 100 m long and 100 m down-dip (Fig. 2b, c) which are spread along the Imiter fault zone (Main quarry, B3 Hill, shaft IV, Igoudrane; Fig. 2a). Supergene alteration is limited to the upper levels of the deposit and is characterized by iron hydroxides developed at the expense of sulfide minerals and cerussite surrounding galena crystals. No supergene sulfide mineral enrichment is observed in the Imiter deposit.

The Imiter fault zone and associated medium- to small-scale structures appear to have focused the mineralizing fluids and controlled silver deposition. A previous microstructural analysis of the mining area (Ouguir et al. 1994) revealed a two-stage kinematic history: (1) NNW extension evolving towards (2) a sinistral extensional movement producing the present-day rhombic geometry of the fault zone (for example, Main quarry in Fig. 2a) and leading to the main mineralization stage. New microstructural analyses conducted during this study (Fig. 3) re-evaluate the kinematic model of Ouguir et al. (1994) and demonstrate the association of silver deposition with two distinct tectonic regimes. The first regime (regime A; Fig. 3) developed normal faults trending N80°E and reflects an extensional direction of N150°E to N180°E. The second tectonic regime (regime B; Fig. 3) was characterized by a subsequent rotation of strain to initiate a sinistral strike-slip regime, leading to reactivation of the NNW–SSE extensional fractures. Regime A appears to be the predominant deformational event in the Imiter area, as it corresponds to down-faulting of the northern block and opening of the major mineralized structures. This regime is associated with the formation of the silver-rich Qtz2 veins and part of the silver-bearing dolomite stage. Regime B is not associated with any major changes in the paragenetic sequence when compared to regime A, except for the presence of dolomite, rather

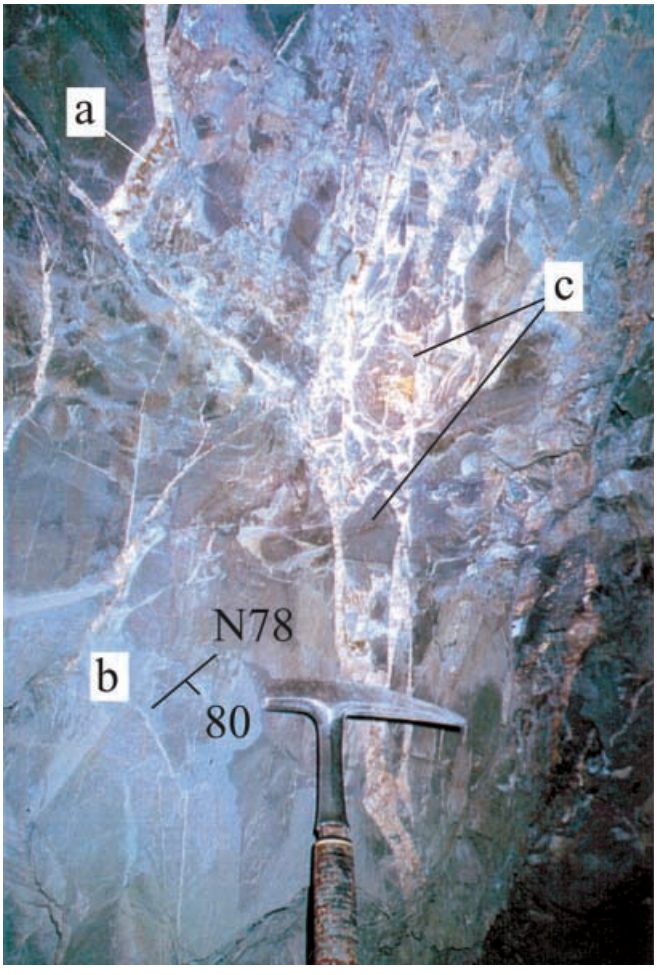

Fig. 4a–c Example of a dolomite-stage vein at Imiter, hosted by the Neoproterozoic black shales. Hydraulic fracturing on a normal fault is clearly visible. **a** Native silver dolomite vein; **b** fault plane (N78°E–80 N); **c** hydraulic breccia

than quartz, as the main gangue mineral. Several rhyolitic dikes are observed underground in the mineralized bodies of the B3 Hill (Fig. 2b). Some dikes are emplaced in the E–W normal faults which are related to regime A. They contain sulfide minerals (mainly pyrite) from Qtz2 stage and rare silver mineralization.

U/Pb geochronology

Zircons from the Taouzzakt granodiorite and Takhatert protrusion were selected for dating the two major magmatic events of the Imiter area. In-situ analyses were carried out at the Centre de Recherches Pétrographiques et Géochimiques using the IMS 1270 Cameca ion probe. The analyzed zircons are small (< 100 μm), and prismatic or needle-shaped. They show a regular, fine magmatic zonation and have no inherited core (Fig. 5). Concordia diagrams for zircons are shown in Fig. 5; errors represent analytical precision at 1σ (see Deloule et al. 2001 for a complete description of the analytical procedure).

Taouzzakt granodiorite

Sixteen analysis were performed on single zircon grains (Fig. 5). The $^{207}Pb/^{235}U$ and $^{206}Pb/^{238}U$ ages are discordant in most cases. The $^{206}Pb/^{207}Pb$ ages plotted on the concordia diagram (Fig. 5) yield three different groups. Two comprise discordant ages between 579 ± 4 Ma and 569 ± 4 Ma (weighted mean age 573 ± 4 Ma; MSWD = 2.6; $n = 4$), and 677 ± 6 Ma and 653 ± 3 Ma. The third group consists of discordant ages defining a discordia line with an upper intercept at 572 ± 5 Ma (MSWD = 0.6; $n = 11$), which is consistent with the age defined by the first group of four ages (573 ± 4 Ma). This age is considered to be the emplacement age of the Taouzzakt granodiorite. The lower intercept of the discordia cuts the concordia near the origin, suggesting lead loss during the later emplacement of the younger Takhatert intrusion. The two concordant ages at ca. 680 Ma were obtained on magmatic zircons with no inherited core. Therefore, they may represent xenocrysts from an earlier Pan-African tectono-metamorphic event during arc-continent collision (ca. 680–600 Ma; Clauer 1974; Leblanc and Lancelot 1980).

Takhatert rhyolite

Twenty-two analyses provided subconcordant $^{206}Pb/^{207}Pb$ ages dispersed between 650 Ma and 550 Ma (Fig. 5). The $^{206}Pb/^{238}U$ and $^{207}Pb/^{235}U$ ages are concordant. The higher intrinsic error on $^{207}Pb/^{235}U$ ages than for $^{206}Pb/^{238}U$ values yield elliptical representative points in the concordia diagram (Fig. 5). Indeed, the $^{207}Pb/^{235}U$ ages are most sensitive to a common lead contribution because the ^{207}Pb ion signal is about 10 times lower than the ^{206}Pb ion signal. Therefore, the individual $^{206}Pb/^{238}U$ ages appear more reliable. Ion-probe data on selected zircons define a geochronologically homogeneous group consisting of nine analyses with the youngest ages (Fig. 5). Slight dispersion of $^{207}Pb/^{235}U$ ages is probably due to the higher uncertainty of the ^{207}Pb ion signal (see above). These nine magmatic zircons yield a weighted mean age of 550 ± 3 Ma which is interpreted as the emplacement age of the rhyolite. This age appears in good agreement with the stratigraphic position of the rhyolite because it is younger than the age of the volcanic rocks at the top of the Neoproterozoic series dated at 563 ± 5 Ma (U/Pb on zircon populations; Mifdal and Peucat 1985) and older than the middle Cambrian rocks in Morocco dated at 517 ± 2 Ma (U/Pb on monozircon; Landing et al. 1998).

Thirteen other zircon grains yield concordant ages scattered between 647 ± 3 Ma and 560 ± 2 Ma. They probably represent xenocrysts inherited from older country rocks (e.g., granitoids and late Neoproterozoic volcanic rocks). Particularly relevant to this group are the ages at ca. 570 Ma corresponding to the age determined for the Taouzzakt granodiorite in contact with the Takhatert rhyolite. Two ages at ca. 650 Ma, and one age at 598 ± 4 Ma could represent xenocryst zircon ages from plutonic rocks belonging to the earlier Pan-African events.

$^{40}Ar/^{39}Ar$ geochronology

Sampling and analytical procedure

New $^{40}Ar/^{39}Ar$ dating was performed on four muscovite samples (IM98-03, IM00-53, IM99-37, IM99-58) selected from the mineralized bodies. Microscopic and SEM analyses on large Ms1 from samples IM00-53, IM99-58 and IM99-37 revealed several microcracks, cleavage openings and recrystallization domains on the rims of the grains or in the cleavage planes. Muscovite separates were obtained by hand-picking. Due to the smaller size of the Ms2 muscovites compared to Ms1, large crystals suitable for individual $^{40}Ar/^{39}Ar$ grain analysis (1 to 4 mm in size) consist of muscovite Ms1. However, it is possible that smaller Ms2 crystals were also selected together with the larger Ms1 grains. This is confirmed by microscopic and SEM analyses on Ms1 grains from samples IM00-53, IM99-58 and IM99-37, which reveal complex morphological features such as microcracks, cleavage openings and recrystallization domains on the rims of the grains or in the cleavage planes. These are usually interpreted as reflecting a polyphase history for the host mineral.

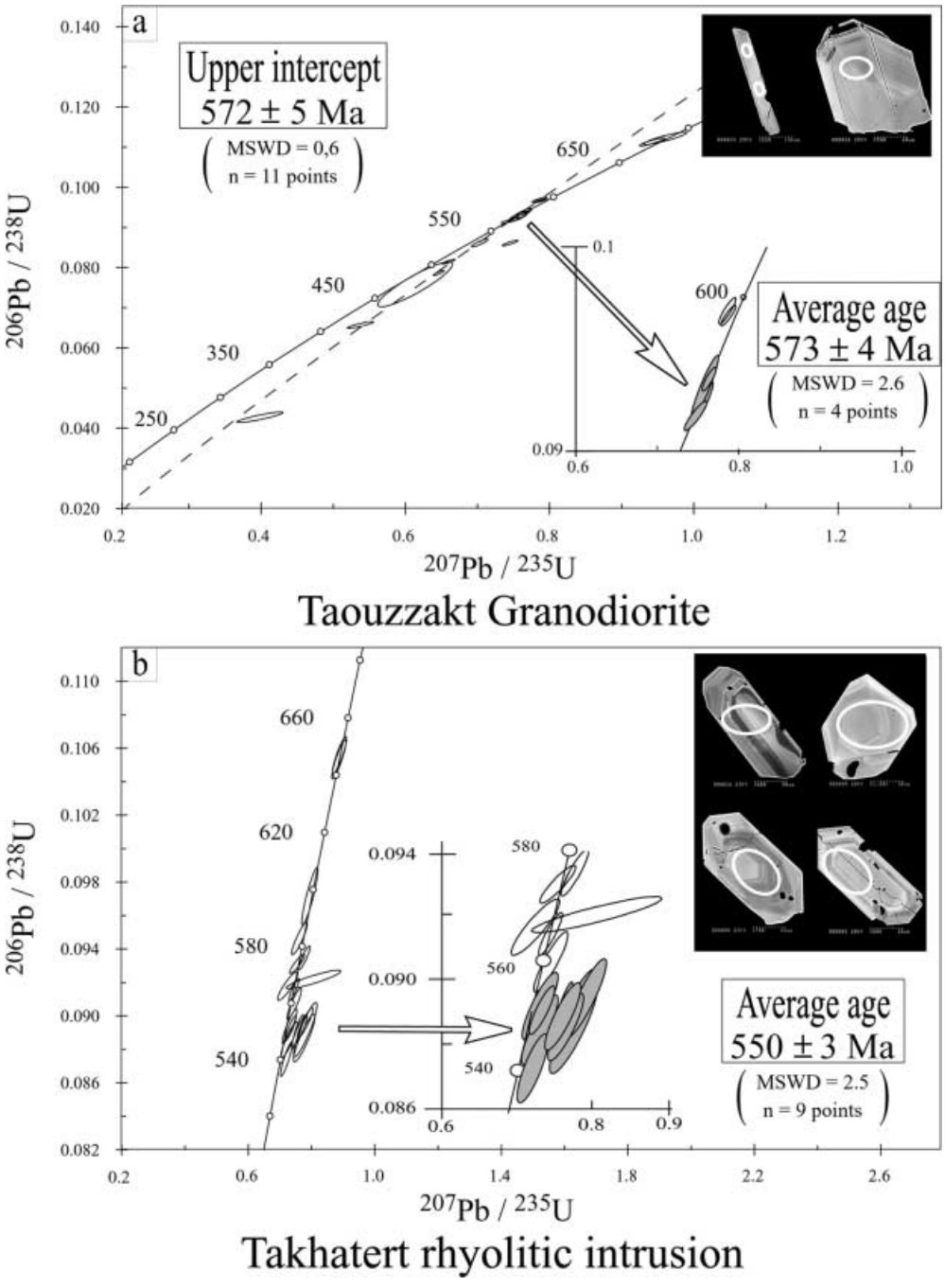

Fig. 5a, b $^{206}Pb/^{238}U$ versus $^{207}Pb/^{235}U$ plot of zircon ion microprobe analysis (Cameca IMS 1270) for the Taouzzakt granodiorite (**a**) and the Takhatert rhyolite (**b**). Ages are calculated with the Isoplot program (Ludwig 2000). The open *ellipses* drawn on the SEM images (*insets*) are examples of spot positions in the analyzed zircon grains

Samples IM98-03 and IM00-53 were obtained from the B3 Hill workings at the 1,279- and 1,335-m levels, respectively, along the contact between the black shales and the granodiorite. These samples are Qtz1 from quartz veins corresponding to the base-metal episode characterized by large Ms1 flakes (> 0.5 cm) and Chl1. In sample IM00-53, Qtz1 shows a graphitic texture. Electron microprobe analysis of Ms1 yields a muscovite composition in the Si/Al diagram (Fig. 6). Estimated crystallization temperatures were obtained using the Monier and Robert (1986) geothermometer. For Ms1 in sample IM00-53, they range from 550 to 650 °C (Fig. 6).

Sample IM99-37 was selected from a quartz–carbonate–chlorite vein hosted in the black shales from the 1,320-m level in shaft IV. The grade is more than 3,000 g/t Ag in this area. Petrographic analysis shows the presence of Qtz1, Chl1, Ms1 and pyrite, corresponding to the base-metal episode, and Ms2 dolomite belonging to the epithermal silver mineralization episode (Fig. 6). The Ms2 occurs as very small crystals (< 100 μm) growing on Chl1. Microprobe analyses of Ms1 and Ms2 from sample IM99-37 yield contrasting compositions spread along the muscovite–phengite line. This variation in composition is also illustrated by a difference in crystallization temperatures, at about 450 °C (Ms1) and 350 °C (Ms2), respectively (Fig. 6).

Sample IM99-58, from a Qtz1–Chl1–pyrite–sphalerite vein from the 1,325-m level in the B3 Hill workings, is also representative of the base-metal episode. In this sample, Ms1 is characterized by small crystals (< 0.5 mm) included within Qtz1 or filling intergranular spaces. The crystallization temperature determined on Ms1 is about 600 °C (Fig. 6). In this area, grades reaching 1,500 g/t Ag have been measured.

During this study, two complementary experimental procedures were applied because of the complexity of the dated material and resulting $^{40}Ar/^{39}Ar$ spectra. We analyzed sample IM98-03 on a VG

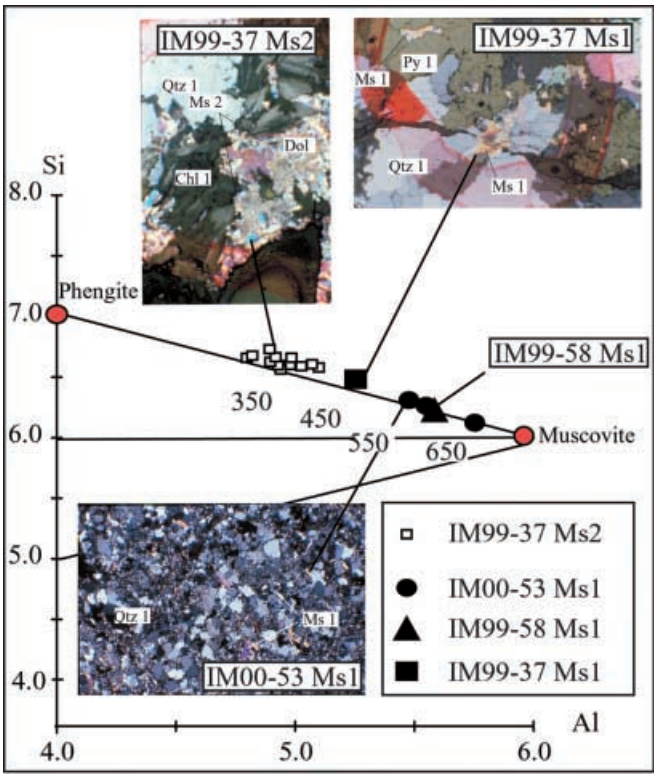

Fig. 6 Characterization of Ms1 and Ms2 muscovites in the Si/Al diagram of Velde (1965; see text for descriptions of the analyzed muscovites; electron-microprobe analysis realized at the UHP University of Nancy, France; Si and Al are represented in a.p.f.u.). Temperatures indicated on the muscovite–phengite line are estimated with the Monier and Robert (1986) geothermometer (see Fig. 3 for abbreviations)

3600 mass spectrometer at the UMR Geosciences-Azur laboratory in Nice (France). Muscovite separates were irradiated in the McMaster University nuclear reactor together with the Hb3gr amphibole (1072 Ma; Roddick 1983) as an irradiation monitor. Step-heating analyses were performed with a laser probe using a Coherent Innova 70-4 continuous argon laser with a maximum output power of 6 W. Mineral grains were analyzed in static mode with a Daly photomultiplier system or a Faraday cage. A complete description of the analytical procedure is given in Ruffet et al. (1997). Errors on age spectra represent analytical precision at a 1 σ level and do not include the errors on the $^{40}Ar^*/^{39}ArK$ ratio and age of the monitor. Muscovites from samples IM99-37, IM99-58 and IM00-53 were analyzed using the MAP 216 mass spectrometer at Queen's University (Kingston, Ontario). Muscovite separates were wrapped in aluminum foil and irradiated along with an intralaboratory standard at the McMaster University nuclear reactor (Hamilton, Ontario). Resulting $^{40}Ar/^{39}Ar$ isotopic data were obtained either by step-heating until fusion using a defocused, 8-W Lexel 3500 continuous argon laser or by spot fusion. Complete analytical procedures are outlined in Clark et al. (1998). Errors for individual steps and the age spectrum plots represent the analytical precision at a 2 σ level, assuming the errors in the ages of the flux monitors (i.e., standards) are zero. A conservative estimate for the error in the J value is 0.5%. This is suitable for comparing within-spectrum variation.

Results of $^{40}Ar/^{39}Ar$ dating

The four resulting age spectra are presented in Fig. 7. They all present irregularities precluding any simple, plateau age calculation. However, two of them, IM99-37 and IM00-53, show a characteristic, saddle-shaped age spectrum which can be interpreted as reflecting a disturbed argon isotopic system due to partial recrystallization of muscovite (Cheilletz et al. 1999; Castonguay et al. 2001; Alexandrov et al. 2002). This interpretation is confirmed by laser-spot analyses of a single grain of IM00-53 muscovite which reveal two groups of ages at approximately 560–565 and 535–550 Ma. This younger group of ages also corresponds to a peculiar area of the muscovite grain (Fig. 8) characterized by a greyish color and microcracks, thus corroborating the existence of localized mineralogical perturbations in the analyzed samples.

Additional information can be obtained from IM98-03 and IM99-58 age spectra which display the classical shape characterizing argon loss by diffusion, as described by Turner (1968) and McDougall and Harrison (1988). The most detailed spectrum, IM98-03, shows a group of ages at 542–552 Ma in the low-temperature steps, followed by a regular increase of apparent ages up to 573 Ma in the high-temperature steps, suggesting a two-stage history for this sample. Petrographic and microprobe analyses of muscovite grains from the Imiter deposit reveal that recrystallization included secondary overgrowth of Ms2 grains on larger Ms1 flakes (Fig. 6). Such recrystallization best explains the observed $^{40}Ar/^{39}Ar$ saddle- or staircase-shaped, disturbed age spectra.

In summary, $^{40}Ar/^{39}Ar$ results indicate the existence of two distinct events. The oldest one is revealed by the high-temperature apparent ages ranging from 577 ± 4 Ma to 563 ± 5 Ma, in good agreement with the U/Pb emplacement age obtained for the Taouzzakt granodiorite (572 ± 5 Ma). These ages also represent the crystallization age of the Ms1 muscovite developed in the metamorphic halo of the granodiorite. Additionally, the low-temperature apparent ages (542–552 Ma) of sample IM98-03 and the intermediate-temperature apparent age minima (540–555 Ma) of the saddle-shaped age spectra of samples IM99-37 and IM00-53 reflect a partial isotopic resetting during recrystallization of Ms1 and crystallization of Ms2. These apparent ages are in good agreement with the 550 ± 3 Ma U/Pb age determined for the Takhatert rhyolitic intrusion, suggesting synchronism of the epithermal silver-rich episode and this magmatic event.

Conclusions

Arguments which favor synchronous rhyolitic volcanism and epithermal silver mineralization at 550 Ma include (1) the emplacement of rhyolitic dikes and formation of the silver mineralization along E-W-trending normal faults during tectonic regime A; (2) the lack of subsequent volcanism in the Imiter area; (3) the necessity of magmatism coeval with mineralization to induce the circulation of the ore-forming fluid (Sillitoe 1993); and (4) the sealing of both rhyolitic volcanism and silver mineralization by the middle Cambrian sedimentary rock cover.

The occurrence of precious- and base-metal anomalies in surrounding rocks of the Imiter deposit (black shales and late Neoproterozoic volcanic and plutonic rocks) constitutes part of an epigenetic alteration halo, rather than a syngenetic pre-concentration as previously interpreted by Vargas (1983), Guillou et al. (1988) and Popov (1995). Muscovite (this study) and fluid-inclusion (Baroudi et al. 1999) geothermometry indicate temperatures of formation of silver mineralization ranging between 290 and 350 °C. These temperatures are compatible with subsurface development of the Imiter deposit approximately 1.5 km from an important, volcanic eruptive center (Takhatert rhyolite intrusion). The lack of an acidic wall-rock alteration halo and the presence of dominantly dolomitic gangue indicate relatively neutral ore fluids.

Part of the Imiter mineralization appears as a telescoped deposit, characterized by a Pb-, Zn-, and Cu-rich episode prior to the economic epithermal silver event. The base-metal episode is associated with the development of a first generation of quartz veins (Qtz1) within the metamorphic halo of the Taouzzakt granodiorite. The ca. 572-Ma age of the intrusion is synchronous with crystallization of Ms1 hydrothermal muscovite. The intrusion formed in

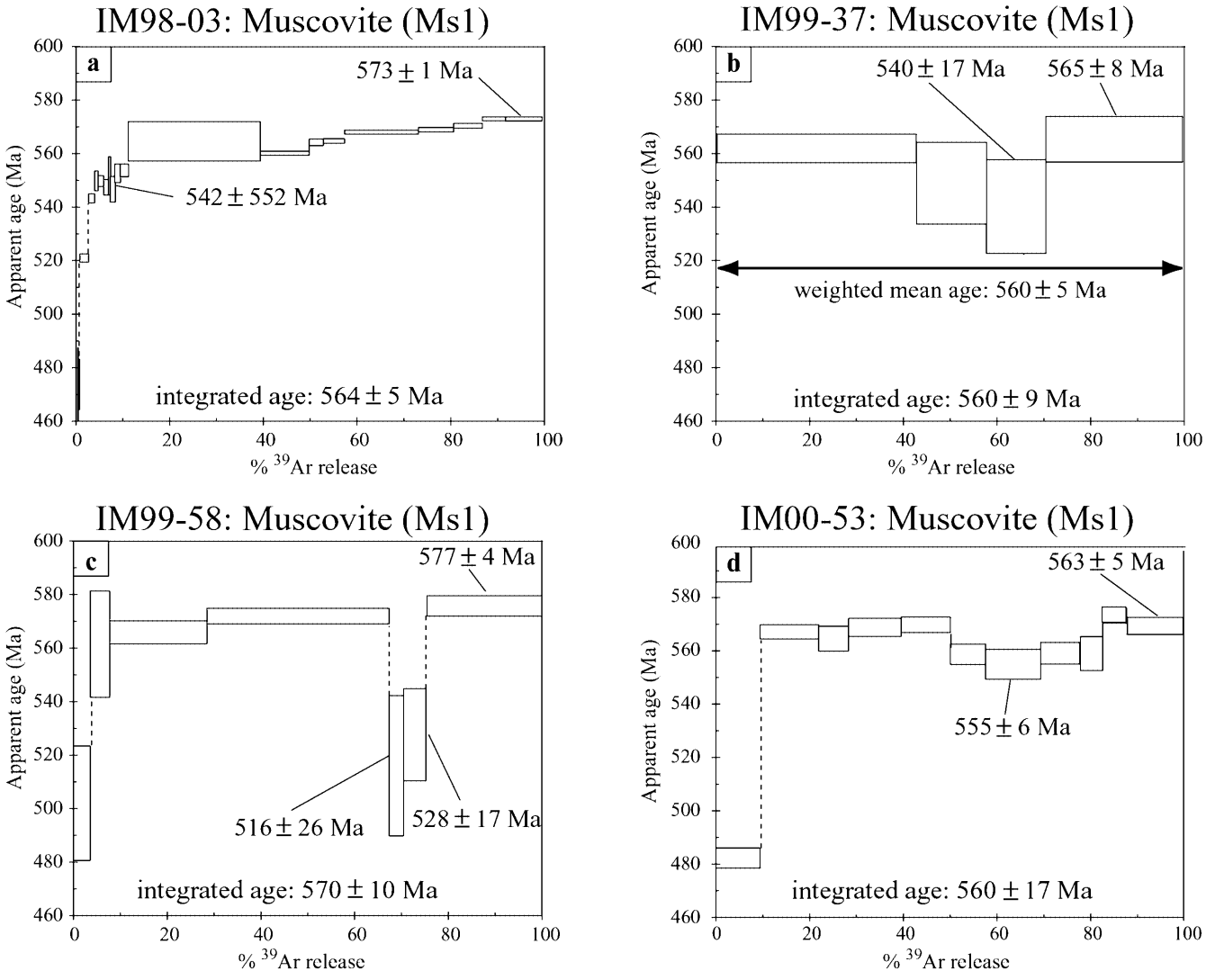

Fig. 7a–d $^{40}Ar/^{39}Ar$ spectra for single crystal, muscovite Ms1 laser step-heating analysis. **a, c** Staircase spectrum illustrating partial resetting of Ms1 crystallization age (right side of the spectrum) by a younger event (left side of the spectrum). **b, d** Saddle-shaped aspect of the low- to medium-temperature steps illustrating different amounts of partial recrystallization of Ms1 and crystallization of Ms2

an active continental margin which was characterized by calc-alkaline magmatism and foreland basin development. The 550-Ma Takhatert rhyolite, the Imiter fault system and the associated epithermal silver ore developed later during a major change from compression to extension in the Pan-African orogen. The silver episode, tentatively dated at ca. 550 Ma at Imiter, is definitively bracketed between the 563-Ma age of the top of the late Neoproterozoic volcanic series in the central Anti-Atlas (Mifdal and Peucat 1985) and an age of 543.9 ± 0.2 Ma for the Precambrian–Cambrian transition (Landing et al. 1998). In the Anti-Atlas domain, this interval corresponds to the so-called Adoudounian (late Neoproterozoic to early Cambrian) transgressive episode (Benziane et al. 1983; Chbani et al. 1999; Piqué et al. 1999) which was characterized by extensional tectonics which could have allowed brines to flow along normal faults developed along the continental shelf of the passive margin. This tectonic setting could account for the presence of highly saline, fluid inclusions in major precious-metal deposits of the Anti-Atlas (Fig. 1): Imiter (Baroudi et al. 1999), Zgounder (Essaraj et al. 1998), Bou Azzer (En-Naciri et al. 1997),

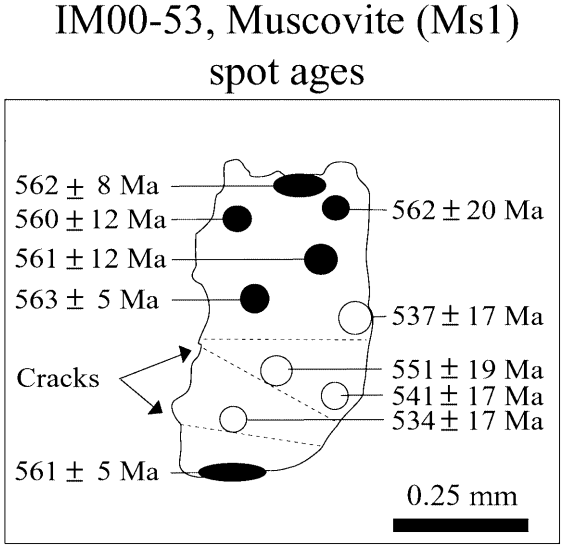

Fig. 8 Laser spot-fusion analysis of a muscovite Ms1 from sample IM00-53

Tiouit (Al Ansari and Sagon 1997), and Bou Madine (Abia et al. 1999).

In the Anti-Atlas, the Precambrian–Cambrian transition appears as an important period for the formation of major, productive precious-metal deposits (Cheilletz and Gasquet 2001). It corresponds to the time of progressive collapse of the Pan-African passive continental margin and a transgression leading to deposition of the early Paleozoic sedimentary rock series. This period is characterized by major tectono-volcanic events occurring during extensional tectonics and was, therefore, highly favorable for shallow melt emplacement (Chalot-Prat and Girbacea 2000), hydrothermal fluid circulation, and associated precious-metal ore formation (Lister et al. 1986). The latter includes formation of the Imiter silver deposit which constitutes a Precambrian analogue to modern epithermal systems (Corbett and Leach 1995).

Acknowledgements This study was supported by several scientific cooperation grants to A.C. and D.G. from the REMINEX-SMI-groupe ONA (Morocco) and the Ministry of Industry (France; #98 2 24 00 30 and #00 224 0002). Zircon ion-probe analysis were carried out under the supervision of E. Deloule, M. Champenois and D. Mangin. The $^{40}Ar/^{39}Ar$ analyses would not have been possible without generous facilities provided by E. Farrar (Queen's University, Kingston, Canada) and G. Féraud (UMR Géosciences-Azur, Nice, France). R.J. Goldfarb, R. Moritz and S. Scaillet are gratefully acknowledged for critical reviews of an early version of the manuscript. Sincere thanks go to G. Dagallier, J. Macaudière, H. Ouguir and R. Ruffet for fruitful discussions. A. Belkabir and M. Jebrak are also thanked for their reviews. Constructive observations and careful English changes by an anonymous associate editor significantly improved the manuscript. Analytical results for U/Pb and Ar/Ar dating are available on request to the first author (A.C.).

References

Abia EH, Nachit A, Ibhi A, Baroudi Z (1999) Les minéralisations filoniennes à Pb, Zn, et Cu de la Boutonnière de l'Ougnat. Relations avec les déformations et essai de calage chronologique. Chron Rech Min 536:83–95

Al Ansari A, Sagon JP (1997) Le gisement d'or de Tiouit (Jbel Saghro, Anti-Atlas, Maroc), un système mésothermal polyphasé à sulfures-or et hématite-or dans une granodiorite potassique d'âge protérozoïque supérieur. Chron Rech Min 527:3–25

Alexandrov P, Ruffet G, Cheilletz A (2002) Muscovite recrystallization and saddle-shaped $^{40}Ar/^{39}Ar$ spectra: example from the Blond granite (Massif Central, France). Geochim Cosmochim Acta 66 (in press)

Angelier J, Mechler P (1977) Sur une méthode graphique de recherche des contraintes principales également utilisable en tectonique et en sismotectonique : la méthode des dièdres droits. Bull Soc Géol Fr 19:1309–1318

Azizi-Samir MR, Saquaque A, El Boukhari A (2001) La transition néoprotérozoïque dans l'Anti-Atlas marocain, un continuum géodynamique particulièrement mineralogène. In: Abstr Vol Coll Magmatisme, Métamorphisme et Minéralisations Associées, Marrakech, Maroc, p 6

Barodi B, Belkasmi A, Bouchta R, Qadrouci A (1998) Les minéralisations argentifères du Maroc: cas du gisement d'Imiter. Chron Rech Min 531/532:77–92

Baroudi Z, Beraouz H, Rahimi A, Saquaque A, Chouhaidi M (1999) Minéralisations polymétalliques argentifères d'Imiter Jbel Saghro, Anti-Atlas, Maroc: minéralogie, évolution des fluides minéralisateurs et mécanismes de dépôts. Chron Rech Min 536/537:91–111

Benziane F, Prost AE, Yazidi A (1983) Le passage du Précambrien au Cambrien précoce volcanique et sédimentaire de l'Anti-Atlas oriental; comparaisons avec l'Anti-Atlas occidental. Bull Soc Géol Fr 7(XXV)4:549–556

Castonguay S, Ruffet G, Tremblay A, Féraud G (2001) Tectono-metamorphic evolution of the southern Quebec Appalachians: $^{40}Ar/^{39}Ar$ evidence for Ordovician crustal thickening and Silurian exhumation of the internal Humber zone. Geol Soc Am Bull 113(1):144–160

Chalot-Prat F, Girbacea R (2000) Partial delamination of continental mantle lithosphere, uplift-related crust-mantle decoupling, volcanism and basin formation: a new model for the Pliocene-Quaternary evolution of the southern East-Carpathians, Romania. Tectonophysics 327:83–107

Chbani B, Beauchamp J, Algouti A, Zouhair A (1999) Eocambrian sedimentary record in a distensional and intracontinental basin: the cycle "basal conglomerates-limestones unit-Tikirt sandstones" of the Bou Azzer El Graara area (central Anti-Atlas, Morocco). C R Acad Sci Paris 329:317–323

Cheilletz A, Gasquet D (2001) Specific plate tectonic environments for the Anti-Atlas ore deposits. In: Abstr Vol Coll Magmatisme, Métamorphisme et Minéralisations Associées, Marrakech, Maroc, p 84

Cheilletz A, Ruffet G, Marignac C, Kolli O, Gasquet D, Feraud G (1999) $^{40}Ar/^{39}Ar$ dating of shear zones in the Variscan basement of Greater Kabylia (Algeria). Evidence of an Eo-Alpine event at 128 Ma (Hauterivian-Barremian boundary): geodynamic consequences. Tectonophysics 306:97–116

Cheilletz A, Azizi-Samir MR, Gasquet D, Zyadi R, Levresse G, Ennaciri A, Archibald D, Ouguir H (2000) Le gisement Ag-Hg d'Imiter (Maroc): âge (U/Pb et $^{40}Ar/^{39}Ar$) et contrôle structural des minéralisations. In: Abstr Vol Coll Métallogénie 2000, Nancy, France, pp 39–40

Clark AH, Archibald DA, Lee AW, Farrar AW, Hodgson CJ (1998) Laser probe $^{40}Ar/^{39}Ar$ ages of early- and late-stage alteration assemblages, Rosario porphyry copper-molybdenum deposit, Collahuasu district, I Region, Chile. Econ Geol 93:326–337

Clauer N (1974) Utilisation de la méthode Rb-Sr pour la datation d'une schistosité de sédiments peu métamorphisés: application au Précambrien II de la boutonnière de Bou-Azzer-El Graara (Anti-Atlas, Maroc). Earth Planet Sci Lett 22:404–412

Corbett GJ, Leach TM (1995) S.W. Pacific rim Au/Cu systems: structure, alteration and mineralization. University of British Columbia, Vancouver, Short Course MRDU 17:150

Deloule E, Alexandrov P, Cheilletz A, Laumonier B, Barbey P (2001) In situ U/Pb zircon ages for Early Ordovician magmatism in the eastern Pyrenees, France: the Canigou orthogneisses. Int J Earth Sci (in press). DOI 10.1007/s00531-001-0232-0

En-Naciri A, Barbanson L, Touray JC (1997) Brine inclusions from the Co-As-(Au) Bou Azzer district, Anti-Atlas Mountains, Morocco. Econ Geol 92:360–367

Ennih N, Liegeois JP (2002) The Moroccan Anti-Atlas: the West African craton passive margin with limited Pan-African activity. Implications for the northern limit of the craton. Precambrian Res (in press)

Essaraj S, Boiron MC, Cathelineau M, Banks D, El Boukhari A, Chouhaidi MY (1998) Brines associated to Ag deposition in the Zgounder silver deposit (Anti-Atlas, Morocco). Eur J Mineral 10:1215–1226

Fekkak A, Boualoul M, Badra L, Amenzou M, Saquaque A, El Amrani IE (2000) Origine et contexte géotectonique des dépôts détritiques du groupe néoprotérozoïque inférieur de Kelaat Mgouna (Anti-Atlas oriental, Maroc). J Afr Earth Sci 30(2):295–311

Fekkak A, Pouclet A, Ouguir H, Badra L, Gasquet D (2001) Géochimie et signification géotectonique des volcanites du Cryogénien inférieur du Saghro (Anti-Atlas oriental, Maroc). Geodyn Acta 14:373–385

Gresse PG, de Beer CH, Chevalier LP, de Kock GS, Thomas RJ (2000) Mémoire explicatif de la carte géologique du Maroc au 1/50 000, feuille Tachoukacht. Notes Mém Serv Géol Maroc 393b

Guillou JJ, Monthel J, Picot P, Pillard F, Protas J, Samama JC (1985) L'imitérite, Ag_2HgS_2, nouvelle espèce minérale; propriétés et structure cristalline. Bull Minéral 108:457–464

Guillou JJ, Monthel J, Samama JC, Tijani A (1988) Morphologie et chronologie relative des associations minérales du gisement mercuro-argentifère d'Imiter (Anti-Atlas, Maroc). Notes Mém Serv Géol Maroc 334:215–228

Landing E, Bowring SA, Davidek K, Westrop S, Geyer G, Heldmaier W (1998) Duration of the Early Cambrian: U/Pb ages of volcanic ashes from Avalon and Gondwana. Can J Earth Sci 34:329–338

Leblanc M, Lancelot JR (1980) Interprétation géodynamique du domaine pan-africain (Précambrien terminal) de l'Anti-Atlas (Maroc) à partir de données géologiques et géochronologiques. Can J Earth Sci 17:142–155

Leistel JM, Qadrouci A (1991) Le gisement argentifère d'Imiter (Protérozoïque supérieur de l'Anti-Atlas, Maroc). Contrôles des minéralisations, hypothèse génétique et perspectives pour l'exploration. Chron Rech Min 502:5–22

Levresse G (2001) Contribution à l'établissement d'un modèle génétique des gisements d'Imiter (Ag-Hg), Bou Madine (Pb-Zn-Cu-Ag-Au), Bou Azzer (Co-Ni-As-Au-Ag) dans l'Anti-Atlas marocain. Thèse Doctorat, Institut National Polytechnique de Lorraine, France

Levresse G, Azizi-Samir MR, Cheilletz A, Gasquet D, Zyadi R, Ennaciri A, Archibald D, Ouguir H (2001a) Le gisement Ag-Hg d'Imiter (Anti-Atlas, Maroc): Nouvelles données U/Pb, $^{40}Ar/^{39}Ar$, $d\delta^{34}S$ et microstructurales appuyant le modèle génétique hydrothermal-épithermal. In: Abstr Vol Coll Magmatisme, Métamorphisme et Minéralisations Associées, Marrakech, Maroc, p 97

Levresse G, Cheilletz A, Gasquet D, Azizi-Samir MR, Zyadi R, Ennaciri A, Archibald D, Ouguir H (2001b) Tectonic framework and geochronology of the Imiter silver deposit (Morocco): Ion microprobe U/Pb and $^{40}Ar/^{39}Ar$ results. In: Abstr Vol 11th EUG, Strasbourg, France, p 546

Lister GS, Etheridge MA, Symonds PA (1986) Detachment faulting and the evolution of passive continental margins. Geology 14:246–250

Ludwig KR (2000) Isoplot/Ex 2.49. A geochronological toolkit for microsoft Excel. Berkeley Geochronolgical Center Spec Publ 1a

McDougall I, Harrison TM (1988) Geochronology and thermochronology by the $^{40}Ar/^{39}Ar$ method. Oxford Monographs on Geology and Geophysics 9. Oxford University Press, New York

Mifdal A, Peucat JJ (1985) Datation U/Pb et Rb/Sr du volcanisme acide de l'Anti-Atlas marocain et du socle sous-jacent dans la région de Ouarzazate; Apport au problème de la limite Précambrien-Cambrien. Sci Géol Bull 38:185–200

Monier G, Robert JL (1986) Muscovite solid solutions in the system K_2O-MgO-FeO-Al_2O_3-SiO_2-H_2O: an experimental study at 2 kbar PH_2O and comparison with natural Li-free white micas. Mineral Mag 50:257–266

Ouguir H, Macaudière J, Dagallier G, Qadrouci A, Leistel JM (1994) Cadre structural du gîte Ag-Hg d'Imiter (Anti-Atlas, Maroc); Implication métallogénique. Bull Soc Géol Fr 165:233–248

Ouguir H, Macaudière J, Dagallier G (1996) Le Protérozoïque supérieur d'Imiter, Saghro oriental, Maroc: un contexte géodynamique d'arrière-arc. J Afr Earth Sci 22:173–189

Piqué A, Bouabdelli M, Soulaïmani A, Youbi N, Iliani M (1999) The Late Proterozoic PIII conglomerates of the Anti-Atlas (southern Morocco). Their relationships with the Pan-African orogeny or a Late Proterozoic rifting episode. C R Acad Sci Paris 328:409–414

Popov AG (1995) Gisement argentifère d'Imiter. Etude minéralogique, paragenèse et zonalité du gisement. Rapp Soc Min Imiter, Tinghar, Maroc

Popov AG, Belkasmi A, Qadrouci A (1986) Le gisement argentifère d'Imiter: synthèse géologique, résultats des recherches de 1985 et bilan des réserves au 31/12/1985. Rapp Soc Min Imiter, Tinghar, Maroc

Roddick JC (1983) High precision intercalibration of $^{40}Ar/^{39}Ar$ standards. Geochim Cosmochim Acta 47:887–898

Ruffet G, Gruau G, Ballèvre M, Féraud G, Philipot P (1997) Rb-Sr and $^{40}Ar/^{39}Ar$ laser probe dating of high-pressure phengites from Sesia zone (Western Alps): underscoring of excess argon and new age constraints on the high pressure metamorphism. Chem Geol 141:1–18

Sillitoe RH (1993) Epithermal models: Genetic types, geometrical controls and shallow features. In: Kirkham RV, Sinclair WD, Thorpe RI, Duke JM (eds) Mineral deposit modelling. Geol Assoc Can Spec Pap 40:403–417

Turner G (1968) The distribution of potassium and argon in chondrites. In: Ahrens LH (ed) Origin and distribution of the elements. Pergamon Press, London, pp 387–398

Vargas JM (1983) Etude métallographique des minéralisations mercuro-argentifère d'Imiter. Rapp Fondation Scientifique de la Géologie et de ses Applications, Nancy

Velde B (1965) Phengite micas: Synthesis, stability and natural occurrences. Am J Sci 263:886–913

Villeneuve M, Cornée JJ (1994) Structure, evolution and palaeogeography of the West African craton and bordering belts during the Neoproterozoic. Precambrian Res 69:307–326